ELSEVIER

Chemical Engineering Science 60 (2005) 4661–4677

Chemical Engineering Science

www.elsevier.com/locate/ces

Effects of feed tray locations to the design of reactive distillation and its implication to control

Yu-Cheng Cheng, Cheng-Ching Yu*

Department of Chemical Engineering, National Taiwan University, Taipei 106-17, Taiwan

Received 5 September 2004; received in revised form 3 February 2005; accepted 14 March 2005
Available online 13 May 2005

Abstract

The effects of feed locations to the design of reactive distillation are explored. In this work, ideal reactive distillation systems are used to illustrate the advantage of feed trays optimization in design and control. Process parameters such as relative volatilities between reactants, relative volatilities between products, column pressure, activation energies, and pre-exponential factors are varied to seek possible generalization. For all systems studied, the percentage of energy saving ranges from 6% to 47%, and this is obtained by simply rearranging the feed locations. Finally, the idea of optimal feed trays is extended to the operation/control of reactive distillation systems. First, steady-state analysis is carried out to find the optimal feed trays as measurable load variable varies. Then, a control structure is proposed to rearrange the feeds as the disturbance comes into the system. The results indicate that, again, substantial energy can be saved by feed rearrangement via the coordinated control structure.

Keywords: Reactive distillation; Feed tray; Control structure design

1. Introduction

The reactive distillation combines both chemical reaction and multicomponent separation into a single unit. It offers significant economic advantages in some systems, particularly when reactions are reversible or when the presence of azeotropes makes conventional separation systems complex and expensive. The applications of reactive distillation in the chemical and petroleum industries have increased rapidly in the past decade (Taylor and Krishna, 2000; Doherty and Malone, 2001). A number of papers and patents have explored the RD systems. The literature up to 1992 was reviewed by Doherty and Buzad (1992). Most of the papers were discussed by steady-state design and optimization problems. Only a few papers studied the dynamic of reactive distillation or the interaction between design and control. Recent books by Doherty and Malone (2001) and Sundmacher and Kienle (2003) present detailed discussions of the technology and its current status. The literatures state that the most common applications of reactive distillation are etherification and esterification reactions. Most of these papers focus on real chemical systems, and each system has its own set of complexities in vapor–liquid equilibrium nonideality (azeotropes), reaction kinetics, physical properties, etc. The discrete nature of chemical species and specific complexities in the VLE seems to cloud the picture in understanding reactive distillation systems. On the other hand, the ideal reactive distillation of Luyben (2000) and Al-Arfaj and Luyben (2000) seems to offer a continuous spectrum in studying the process behavior by stripping away all the non-ideal VLE and specific reaction rates. Only a limited number of papers study the ideal reactive distillation systems. Al-Arfaj and Luyben (2000) studied the control of an ideal two-product reactive distillation system. Simple ideal physical properties and kinetics are assumed so that the control issue can be explored without being clouded by complexities of a specific chemical system. Sundmacher and Qi (2003) also compare the conceptual design of reactive distillation process

* Corresponding author. Tel.: +886 2 3365 1759; fax: +886 2 2362 3040.
E-mail address: ccyu@ntu.edu.tw (C.-C. Yu).

0009-2509/$ - see front matter © 2005 Elsevier Ltd. All rights reserved.
doi:10.1016/j.ces.2005.03.033

configurations for ideal binary mixtures, and comparisons are made to the conventional process. A recent paper by Kaymak and Luyben (2004) also makes quantitative comparisons of simple reactive distillation for different chemical equilibrium constants and relative volatilities (Kaymak et al., 2004).

The reactive distillation differs from the conventional distillation in that a tubular type of reactor, the reactive flash cascades to be specific (Doherty and Malone, 2001), is cascaded with separation units. From this perspective, the composition profile inside the reactive zone becomes important for an effective operation of the reactive flash cascades. Moreover, typical distillation columns follow certain temperature profile. That is, the temperature increases as one steps down the column. The *composition* as well as the *temperature* effects should play some role for the performance of a reactive distillation column. The reactant feed location is an obvious design degree of freedom to locate optimal composition and temperatures profiles inside the column. It then becomes obvious that the feed tray location should be included as a design variable. Therefore, the objective of this work is to explore the effects of feed tray location to the performance of reactive distillation systems.

In this work two types of chemical systems are studied. One is systems with larger activation energies (temperature sensitive reaction) and the other is systems with smaller activation energies. For each type, the effects of relative volatilities between reactants and between products are also studied. The results clearly indicate that it is necessary to rearrange the feed tray locations to obtain optimal design (i.e., minimum energy consumption). Qualitative explanations to the shifting in the feed locations are also given. Furthermore, the optimal feed locations also vary as the capacity of the column is changed. This mimics the scenarios of the catalyst deactivation and/or production rate increases. Therefore, the optimized feed tray location can be extended to the operation aspect of reactive distillation systems. Control structures are devised to maintain optimal composition and temperature profiles as operating condition changes.

2. Process studies

Consider an ideal reactive distillation (Fig. 1) with a reversible liquid-phase reaction in the reactive section.

$$A + B \Leftrightarrow C + D.$$

The forward and backward specific rates following the Arrhenius law on tray j are given by

$$k_{Fj} = a_F e^{-E_F/RT_j}, \quad (1)$$

$$k_{Bj} = a_B e^{-E_B/RT_j}, \quad (2)$$

where a_F and a_B are the pre-exponential factors, E_F and E_B are the activation energies, and T_j is the absolute temperature

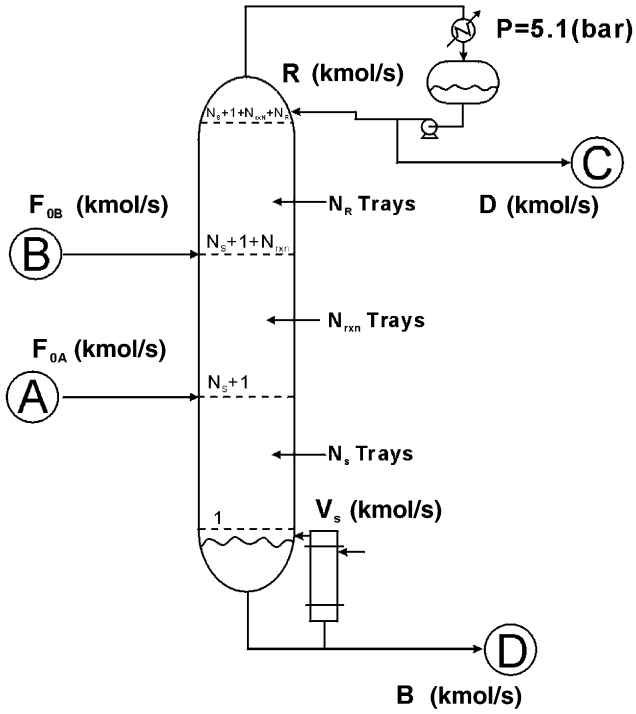

Fig. 1. The reactive distillation with N_R rectifying trays, $N_{r\times n}$ reactive trays, and N_S stripping trays under conventional feed arrangement ($N_{F,B} = N_{r\times n,\text{top}}$ and $N_{F,A} = N_{r\times n,\text{bot}}$).

on tray j. The reaction rate on tray j can be expressed in terms of mole fractions ($x_{j,i}$) and the liquid holdups (M_j).

$$R_{j,i} = v_i M_j (k_{Fj} x_{j,A} x_{j,B} - k_{Bj} x_{j,C} x_{j,D}), \quad (3)$$

where $R_{j,i}$ is the reaction rate of component i on the jth tray (kmol/s), v_i is the stoichiometric coefficient which takes a negative value for the reactants, and M_j is the kinetic holdup on tray j (kmol) and takes a constant value throughout the simulation (This is typically true for catalyst weight based kinetics.)

The assumptions made in this work include:

(1) The forward reaction rate is specified as 0.008 kmol/s at 366 K, and k_B is set to 0.004 kmol/s at the same temperature. Kinetic and physical property data for the system are given in Table 1 (Al-Arfaj and Luyben, 2000).
(2) The kinetics holdup (M_j) of 1000 moles is assumed (Al-Arfaj and Luyben, 2000).
(3) Ideal vapor–liquid equilibrium is assumed, in which constant relative volatilities are used. The tray temperature is computed from Antoine vapor pressure equation (Table 1). Note that as the result of constant relative volatility, the Antoine coefficients, B_{VP}'s , are the same for all four components.
(4) Vapor holdup and pressure drop are neglected.

As shown in the Fig. 1, the column is divided into three sections. The first one is the reactive section containing $N_{r\times n}$ trays. The rectifying section (which is above the reactive

Table 1
Physical properties for the high activation energies case

Activation energy (cal/mol)			Forward (E_F)		30 000
			Backward (E_B)		40 000
Specific reaction rate at 366 K (kmol/s/kmol)			Forward (k_F)		0.008
			Backward (k_B)		0.004
Heat of reaction (cal/mol)					−10 000
Heat of vaporization (cal/mol)					6944
Relative volatilities ($\alpha_C/\alpha_A/\alpha_B/\alpha_D$)					8/4/2/1
		C	A	B	D
Vapor pressure constants[a]	A_{VP}	13.04	12.34	11.45	10.96
	B_{VP}	3862	3862	3862	3862

[a] $\ln P_i^S = A_{VP,i} - B_{VP,i}/T$ where T in Kelvin and P_i^S is the vapor pressure of pure component i in bar.

section) has N_R trays and the stripping section (which is below the reactive zone) has N_S trays. Thus, we are considering a reactive distillation column in which reaction only occurs in the reactive section, which implies a solid-catalysis catalyzed reaction.

The relative volatilities of the components are in the following order:

$$\alpha_C > \alpha_A > \alpha_B > \alpha_D.$$

The products C and D are the lightest and heaviest components, respectively, with the reactants A and B as middle boilers. The thermodynamic behavior indicates that we should remove the product C from the distillate and obtain heavy product D from the bottoms. Fig. 1 also shows that the fresh feed stream F_{OA} containing reactant A is fed to the bottom of the reactive zone, and the heavier reactant B is fed to the top of the reactive zone. Quite volatile as compared to B and D, the light reactant A goes up the column and leaves small traces in the stripping section. Likewise, the heavy reactant B goes down the column, after being fed on the top tray of the reactive zone, and little component B can be found in the rectifying section. Thus, the primary separation in the stripping section is between B and D and in the rectifying section is between C and A.

2.1. Modeling

In Fig. 1, the component balances for the column are expressed as

rectifying and stripping trays:

$$\frac{\mathrm{d}(x_{j,i}M_j)}{\mathrm{d}t} = L_{j+1}x_{j+1,i} + V_{j-1}y_{j-1,i} - L_j x_{j,i} - V_j y_{j,i}. \quad (4)$$

reactive trays:

$$\frac{\mathrm{d}(x_{j,i}M_j)}{\mathrm{d}t} = L_{j+1}x_{j+1,i} + V_{j-1}y_{j-1,i} - L_j x_{j,i} - V_j y_{j,i} + R_{j,i}. \quad (5)$$

feed trays:

$$\frac{\mathrm{d}(x_{j,i}M_j)}{\mathrm{d}t} = L_{j+1}x_{j+1,i} + V_{j-1}y_{j-1,i} - L_j x_{j,i} - V_j y_{j,i} + R_{j,i} + F_j z_{j,i}. \quad (6)$$

Here $x_{j,i}$ and $y_{j,i}$ denote liquid and vapor mole fraction of component i on tray j, with L_j and V_j stands for liquid and vapor flow rates for the jth tray. Liquid hydraulic time constant (β) is included by using a linearized form of the Francis weir formulation, and β is set to 6 s in this work. Since equimolal overflow is assumed, the vapor and liquid flow rates are constant throughout the stripping and rectifying sections, except for the reactive zone as a result of an exothermic reaction (Al-Arfaj and Luyben, 2000). The heat of reaction vaporizes some liquid on each tray in this section. Therefore the vapor flow rate increases up through the reactive zone, while the liquid flow rate decreases down through the reactive zone:

$$V_j = V_{j-1} - \frac{\lambda}{\Delta H_v} R_{j,i}, \quad (7)$$

$$L_j = L_{j+1} + \frac{\lambda}{\Delta H_v} R_{j,i}, \quad (8)$$

where λ is the heat of reaction (−10 000 cal/mol) and ΔH_v is the latent heat of vaporization (6944 cal/mol).

The vapor–liquid equilibrium is assumed to be ideal and the bubble point temperature calculation is used to find the tray temperature (see Table 1 for the vapor pressure data of pure component).

$$P = x_{j,A}P^S_{A(T_j)} + x_{j,B}P^S_{B(T_j)} + x_{j,C}P^S_{C(T_j)} + x_{j,D}P^S_{D(T_j)}, \quad (9)$$

where total pressure P and vapor pressures P^S are in bar. The column pressure is fixed at 5.1 bar.

Table 2
Effects of feed locations to design for systems with different relative volatilities and rate constants (temperature sensitive kinetics; $E_F = 30\,000$ and $E_B = 40\,000$ cal/mol)

	Base case	$\frac{\alpha_A}{\alpha_B} = 2$	$\frac{\alpha_A}{\alpha_B} = 1.5$	$\frac{\alpha_A}{\alpha_B} = 3.0$	$\frac{\alpha_C}{\alpha_A} = 4.0$	$\frac{\alpha_B}{\alpha_D} = 4.0$	Optimal P (9 bar)	Low k	High k
$\alpha_C/\alpha_A/\alpha_B/\alpha_D$	**8/4/2/1**	**8/4/2/1**	**6/3/2/1**	**12/6/2/1**	**16/4/2/1**	**16/8/4/1**	8/4/2/1	8/4/2/1	8/4/2/1
$k_{F,366}$ (s^{-1})	**0.008**	0.008	0.008	0.008	0.008	0.008	0.008	**0.0048**	**0.016**
$k_{B,366}$ (s^{-1})	**0.004**	0.004	0.004	0.004	0.004	0.004	0.004	**0.0024**	**0.008**
$N_S/N_{r\times n}/N_R$	8/11/9	8/11/9	9/11/9	8/11/8	5/11/5	6/11/6	8/11/9	8/11/9	6/11/6
$N_{r\times n,\mathrm{bot}}/N_{r\times n,\mathrm{top}}$	**9/19**	**9/19**	**10/20**	**9/19**	**6/16**	**7/17**	**9/19**	**9/19**	**7/17**
$N_{F,A}/N_{F,B}$	**9/19**	**11/15**	**11/13**	**10/17**	**12/14**	**8/10**	**14/17**	**9/17**	**10/13**
$X_{D,C}/X_{B,D}$	0.95/0.95	0.95/0.95	0.95/0.95	0.95/0.95	0.95/0.95	0.95/0.95	0.95/0.95	0.95/0.95	0.95/0.95
F_{OA}, F_{OB}, D, B (kmol/s)	0.0126	0.0126	0.0126	0.0126	0.0126	0.0126	0.0126	0.0126	0.0126
R (kmol/s)	0.0366	0.0332	0.0409	0.0274	0.0198	0.0284	0.0263	0.0445	0.0277
V_S (kmol/s)	0.0320	0.0285	0.0362	0.0227	0.0152	0.0237	0.0217	0.0399	0.0230
Percent energy saving[a] (%)	**0**	**−10.9**	**−15.2**	**−6.9**	**−46.8**	**−15.6**	**−27.1**	**−5.5**	**−21.9**

[a]Compared to the conventional feed arrangement (i.e., $N_{rxn,\mathrm{bot}} = N_{F,A}$ and $N_{rxn,\mathrm{top}} = N_{F,B}$).

2.2. Steady-state design

Typical design variables of a reactive distillation column include: (1) the column pressure P, (2) the number of reactive trays $N_{r\times n}$, (3) the numbers of trays in the stripping and rectifying sections (N_S and N_R, respectively), and (4) the locations of the feed trays ($N_{F,A}$ and $N_{F,B}$, respectively).

In this work, the column pressure P is fixed at a constant value, and the number of reactive trays ($N_{r\times n}$) is selected to ensure the desired conversion with the conventional feed arrangement (heavy reactant to the top of the reactive zone, and the light reactant to the bottom of the reactive zone). The number of trays in the stripping and rectifying sections is set to twice of the minimum number of trays according to the Fenske's Equation (Douglas, 1988), which is

$$N = 2N_{\min} = 2\ln\left(\frac{x_{D,LK}}{x_{D,HK}}\frac{x_{B,HK}}{x_{B,LK}}\right)\Big/\ln\left(\frac{\alpha_{LK}}{\alpha_{HK}}\right), \quad (10)$$

where the subscripts *LK* and *HK* stand for the light key and heavy key, respectively. For the rectifying tray number (N_R), we use the liquid composition right above the reactive tray for x_B, and for N_S, we use the vapor phase composition right below the reactive zone as x_D. This leaves us with the feed tray locations as the design variables. Because all tray numbers are determined, effects of feed tray locations can be compared by simply looking at the energy consumption (i.e., vapor rate).

2.3. Base case

Equations describing the material balances were programmed in FORTRAN code, and all simulations were carried out on Pentium PC. It should be emphasized that the convergence of the reactive distillation is far more difficult than conventional distillation is. Typically, a steady-state simulation is carried out in a two-step procedure. First, the Wang–Henke method is used to converge the flowsheet (MESH equations) to a certain degree (actually to the point at which the objective function fluctuates). Then, the temperature and composition profiles are fed to a dynamic program that is integrated until temperatures and compositions converge.

Saturated liquid feeds were assumed, and two feed flow rates are 0.0126 kmol/s each with pure A ($N_{F,A}$) or B ($N_{F,B}$), which were introduced to the bottom ($N_{r\times n,\mathrm{bot}}$) or the top ($N_{r\times n,\mathrm{top}}$) of the reactive section (see Fig. 1 or base case in Table 2). Note that this is the typical feed arrangement for reactive distillation, which is termed as the *conventional* feed arrangement hereafter. In this work, the conversion is specified to be 95%, and this corresponds to purities of 95% C in the distillation and 95% D in the bottoms.

Fig. 2 (thickest line) shows the composition profiles of all four components at the nominal design. Reactant A has the highest concentration (x_A) on the feed tray ($N_{F,A} = 9$). The profile shows that x_A decreases toward the upper reactive zone as a result of the reaction and also decreases toward the bottoms of the column as a result of separation. Similar behavior is observed for the heavy reactant B (Fig. 2). Both the light product C and heavy product D meet the specification toward the ends of the column.

Luyben and Al-Arfaj (2000) show the steady-state temperature profile at which a non-monotonic temperature profile is observed and at which the local temperature minimum on the lower feed tray is caused by the presence of a significant amount of the light reactant A. This behavior is not uncommon for reactive distillation columns but is rarely seen in the conventional distillation.

2.4. Feed locations versus reactants distribution

It should be emphasized that the reactive section of a reactive distillation column can be viewed as a cascade-type two-phase reactor with the reactor temperature determined

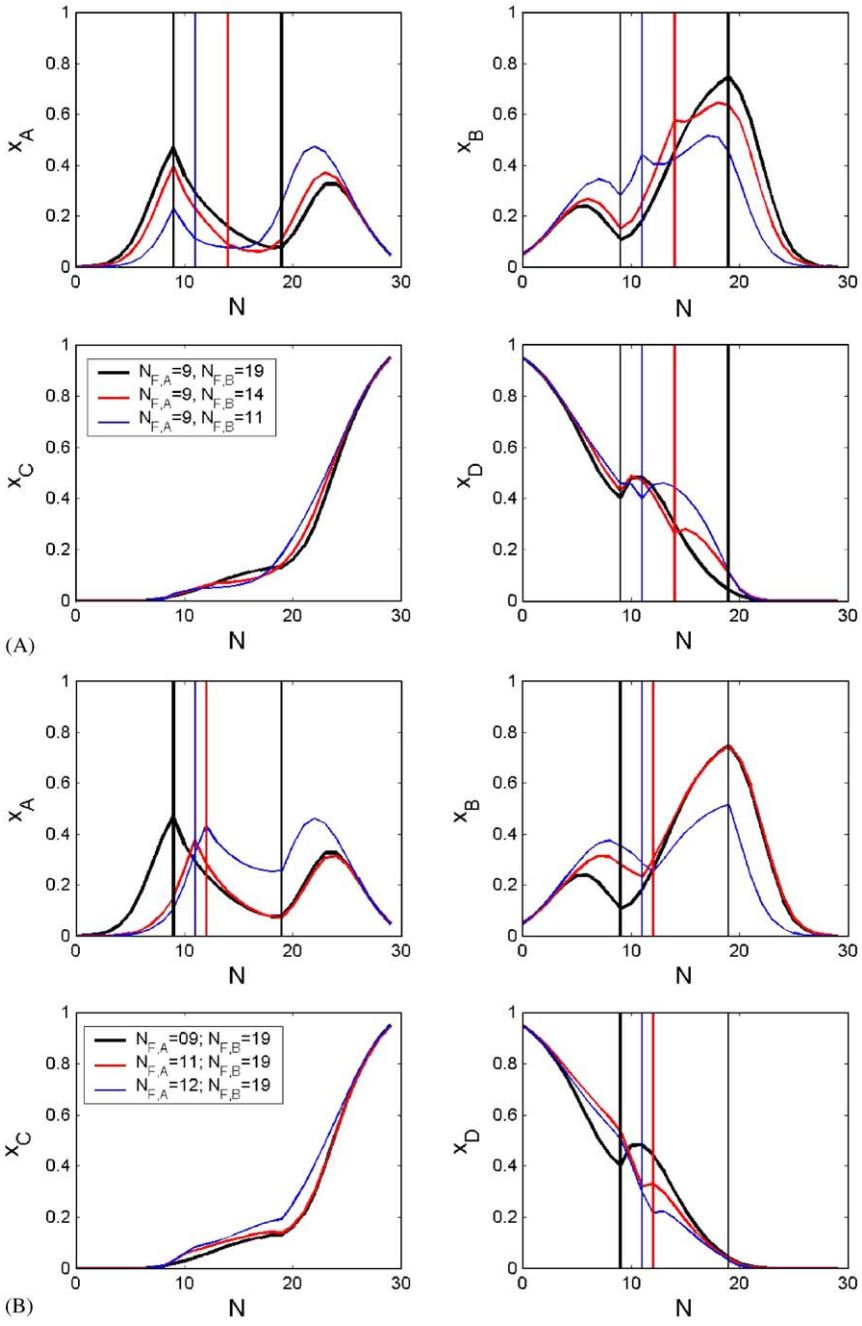

Fig. 2. Composition profiles by changing the feed location of: (A) the heavy reactant B ($N_{F,B}$) and (B) the light reactant A ($N_{F,A}$).

by the bubble-point temperature of the tray liquid phase composition. It is clear that the composition and temperature profiles will certainly affect the performance of the reactive zone, and the feed tray locations appear to be one of the most effective variables for these profiles redistribution. In this section, we are interested in how the composition profile will be affected by changing the feed tray location, and the individual feed tray is changed one at a time.

First we fix the $N_{F,A}$ at the bottom of the reactive zone and change the feed location of the B component from top to bottom. At constant volatilities systems, the feed location of B ($N_{F,B}$) is varied from 19 down to 14 and then to 11 ($N_{F,B} = 19$, 14, or 11). Fig. 2A shows the composition profiles in the column as $N_{F,B}$ changes. As the feed location of component B moves down the column, the mole fraction of heavy reactant B (x_B) increases toward the lower section of reactive zone, as can be seen in Fig. 2A. That means we have a wider and less variation in the distribution of component B throughout the reactive zone as the feed tray is lowered. Consequently, the mole fraction of the light reactant A (x_A) becomes smaller in the lower reactive zone while the profiles of two products (x_C and x_D) remain qualitatively similar as

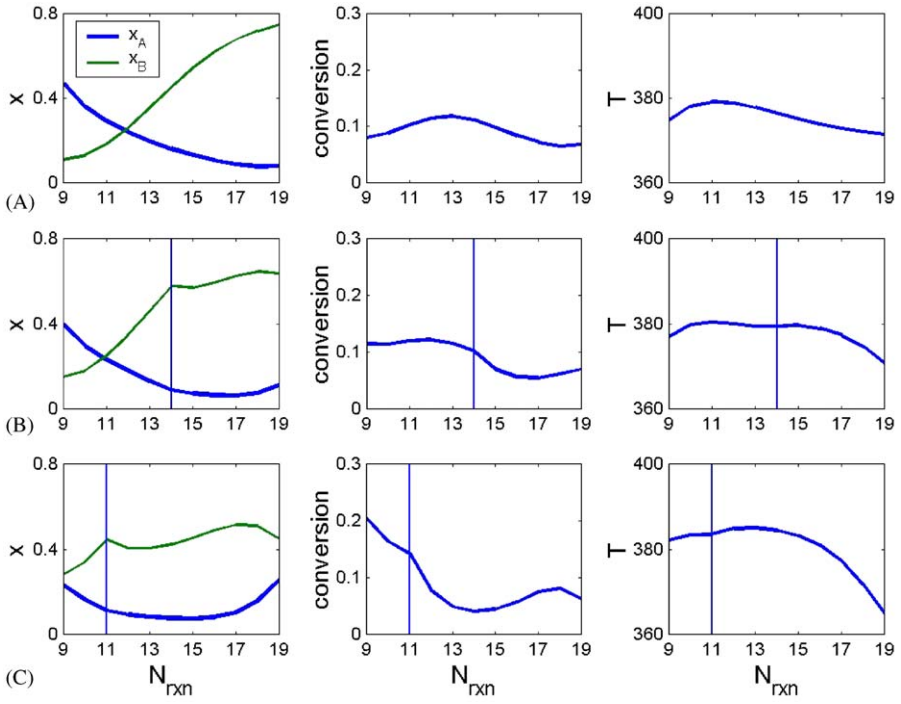

Fig. 3. Reactant composition, fraction of the total conversion, and temperature profiles in the reactive zone by changing the feed location of the heavy reactant B: (A) $N_{F,B} = 19$, (B) $N_{F,B} = 14$, and (C) $N_{F,B} = 11$.

shown in Fig. 2A. This rearrangement of the reactant composition certainly alters the "fraction of total conversion" (i.e., reaction rate in each tray divided by the overall reaction rate) as well as the temperature profile in the reactive zone. Fig. 3 shows the profiles of the fraction of total conversion, of the reactants, and of the temperature in the reactive section as $N_{F,B}$ varies. When we move $N_{F,B}$ down, both the reactant B and conversion increase in the lower reactive section. This implies that the lower reactive trays are better utilized, but at the cost of smaller conversion in the upper reactive trays (i.e., upper reactive trays are underutilized; Fig. 3A–C). It seems a balanced usage of the reactive trays is necessary to achieve optimality and this means an optimal feed location exists for component B. The energy consumption (vapor rate V_S to be exact) is a good measure the column performance. In this case, the vapor rate changes from 0.0320 to 0.0315 and then to 0.0397 (kmol/s) as $N_{F,B}$ changes from 19 down to 14 then to 11. The results clearly indicate that the energy penalty can be significant if one places the feed at an inappropriate location, and the conventional design seems to be a pretty good choice.

The same analysis can be carried over to the feed location of the light component A. Now we fix the $N_{F,B}$ at the top reactive zone (i.e., $N_{F,B} = N_{r\times n,\text{top}}$) by varying $N_{F,A}$. The feed location ($N_{F,A}$) is varied from 9, to 11, and then to 12. Again, Fig. 2B shows that the mole fraction of A increases toward the top of the reactive section (x_A in Fig. 2B) while the mole fraction of the heavy reactant B decreases (x_B in Fig. 2B). However, the heavy reactant B increases toward the bottom of the reactive zone, as can be seen in

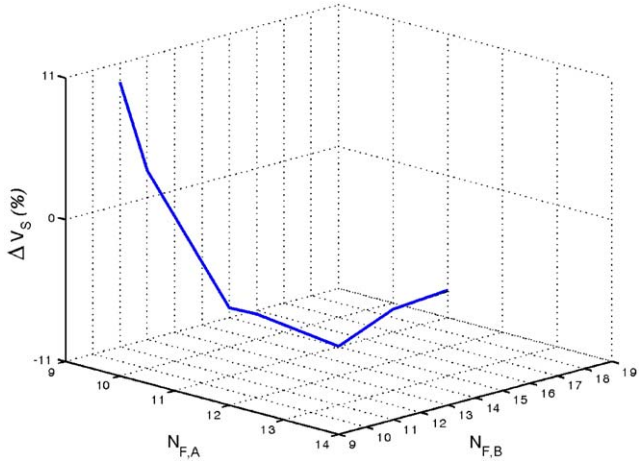

Fig. 4. Feed tray locations and corresponding energy consumption (compared to the base case) throughout the optimization step.

Fig. 2B. This reactant redistribution leads to a significantly different energy consumption, and in the case of variable $N_{F,A}$, the vapor rate changes from 0.0320 to 0.0292 and then to 0.0386 kmol/s as $N_{F,A}$ moves from 9 up to 11, and then to 12.

The on-going analysis clearly indicates that the feed tray locations are important design/operation parameter. Improved process design can be achieved by simply adjusting the feed locations. One question then arises: how much energy can be saved if we adjust the feed locations simultaneously?

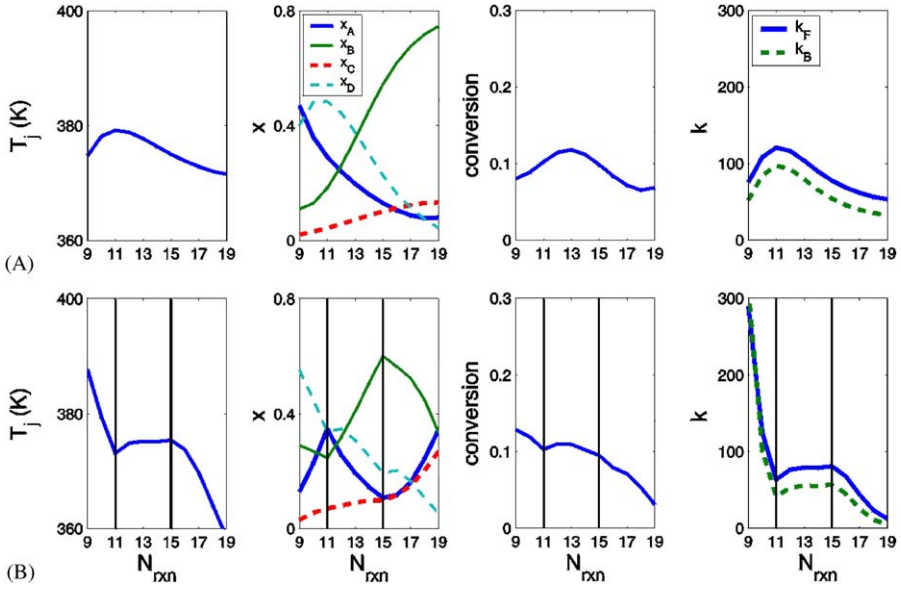

Fig. 5. Profiles of temperature, composition, fraction of total conversion, and reaction rate constant in the reactive zone for the base case with: (A) conventional feed arrangement ($N_{F,A} = 9$ and $N_{F,B} = 19$), and (B) optimal feed arrangement ($N_{F,A} = 11$ and $N_{F,B} = 15$) with 11% energy saving.

2.5. Optimal feed locations

Finding the optimal feed locations can be formulated as an optimization problem in which the vapor rate is minimized by varying the feed tray locations.

$$\begin{aligned} &\underset{N_{F,B},N_{F,A}}{\text{Minimize}} \quad V_S \\ &\text{subject to:} \quad X_{D,C} = X_{B,D} = 0.95. \end{aligned} \tag{11}$$

Because the total tray number (N_T) is finite, one can find the optima by exhausting all N_T^2 possibilities. It is reasonable to restrict the search space to the reactive zone so that the possible choices are further reduced to $N_{r\times n}^2$. In this work, a brute force approach is taken by fixing $N_{F,A}$ first while varying $N_{F,B}$ until a minimum V_S is found. Next, $N_{F,A}$ is changed, and the procedure repeats itself until a global minimum is located. Fig. 4 shows the variation of the vapor rate throughout the process. The results indicate that one should move the feed location of the heavy reactant B down to $N_{F,B} = 15$ (from 19) and move the feed tray of the light reactant A up to $N_{F,A} = 11$ (from 9). This corresponds to a 10.9% energy saving, compared to the conventional feed arrangement (see Table 2). Furthermore, simulation results from this and many other examples reveal that the feed location of the heavy reactant should *not* be placed *lower* then the feed tray of the light reactant. This reduces the search space further down to $(N_{r\times n} + 1)N_{r\times n}/2$.

In addition to the percentage of energy saving, comparisons are also made in terms of profiles of temperature, of composition, of reaction rate on each tray, and reaction rate constants. Fig. 5 shows that the case of optimal feed arrangement (Fig. 5B) has a much *sharper* temperature profile in the reactive zone than the case of conventional feed locations (Fig. 5A). It is also observed that the tray temperature almost reaches 390 K in the former case, while the latter barely reaches 380 K. Furthermore, the profiles of tray conversion and rate constant also take qualitatively similar shape as that of the temperature. The composition profiles in Fig. 5 explain how it happens. First, as the result of moving $N_{F,B}$ downward and $N_{F,A}$ upward, we have non-monotonic *reactant* distributions for the optimal case as opposed to the monotonic *reactant* distribution for the conventional one. This is advantageous for the forward reaction. Next, one obtains an almost monotonic *product* distribution for the optimal case, especially for the heavy product D, and x_D (tray composition of product D) almost reaches 60% at the bottom of the reactive section, which has profound effect on the temperature profile. On the other hand, the mole fraction of D gives a non-monotonic profile for the conventional case, and x_D takes a downturn toward the bottom of the reactive tray as the result of dilution from the excess light reactant A which is introduced on the bottom of the reactive zone. The results presented in Fig. 5 reveal the complicated interaction between temperature and composition in the reactive zone, and it is almost certain that a better profile can always be achieved by varying the feed locations.

In summary, for the system with relative volatilities of $\alpha_C/\alpha_A/\alpha_B/\alpha_D = 8/4/2/1$, one should move the feed locations of the heavy reactant downward and light reactant upward. In terms of the search space for the optimal feed trays, we have the following heuristics:

Heuristic H1. Never place the heavy reactant feed below the feed tray of the light reactant (similarly, do not place the light reactant feed above the feed tray of the heavy reactant).

3. Effects of relative volatilities

Up to now, only one specific example is explored, it will be interesting to see whether the results can be extended to different cases (e.g., different relative volatilities) and how the process change will impact the location of optimal feed trays and the percent of energy saving. Note that for every case studied, the column is *re-designed* using the procedure in Section 3. This means the columns may have different N_R, N_S, and $N_{r\times n}$ and the location of the feed trays are descried in terms of their relative position in the reactive zone.

3.1. Changing relative volatilities of reactants

In this section, we will explore the effects of relative volatilities of reactants to the feed tray locations. By relative volatilities of reactants, we mean that the separation between the two reactants (A and B) becomes easier or more difficult while keeping the relative values of the products constant. Two cases are studied: one is a more difficult separation (i.e., $\alpha_A/\alpha_B = 3/2$) and the other one is an easier one (i.e., $\alpha_A/\alpha_B = 6/2$), compared to the base case (i.e., $\alpha_A/\alpha_B = 4/2$).

In the first case, the relative volatilities are $\alpha_C = 6$, $\alpha_A = 3$, $\alpha_B = 2$, and $\alpha_D = 1$, respectively. With the conventional feed arrangement, we have 33% more energy consumption (0.0428 kmol/s), compared to that of the base case. This shows that, similar to the conventional distillation, difficult separation, even between reactants A and B, requires more energy. Moreover, the composition of A is higher toward the lower reactive zone as compared to the base case (cf. Figs. 5A and 6A) and this leads to a decrease in product D composition which subsequently requires a larger vapor rate to meet the specification. Following the optimization procedure, the result shows the optimum feed trays are $N_{F,A} = 11$ and $N_{F,B} = 13$ (Fig. 6B) which corresponds to a 15.2% energy saving (from 0.0428 to 0.0363 kmol/s) over the conventional feed arrangement (Table 2). It should be emphasized here that the percent of energy saving is computed with respect to the conventional feed arrangement in each case. One immediately observes that the two feeds move *closer* to each other (only two trays apart), and a non-monotonic reactant composition distribution can be seen (Fig. 6B). Similar to the base case (e.g., Fig. 5B), we also have an almost monotonic composition distribution in D. This results in a higher temperature in the lower section of the reactive trays and leads to a higher reaction rate and consequently higher conversion, as shown in Fig. 6B.

The other case is just the opposite where we have easy separation between two reactants. In this example, the relative volatilities are $\alpha_C = 12$, $\alpha_A = 6$, $\alpha_B = 2$, and $\alpha_D = 1$, respectively. Unlike in the previous example, the energy consumption (0.0227 kmol/s) is only 84.4% (0.0227/00320*100%) of the base case. This again reconfirms that well known fact of the conventional distillation—easy separation requires less energy—is also applicable to reactive distillation. It is also observed that the composition of D is higher toward the lower reactive zone as compared to the other two cases (cf. Figs. 5A, 6A), and this implies a smaller vapor rate to meet the specification. The optimization result shows that the optimum feed trays are $N_{F,A} = 10$ and $N_{F,B} = 17$, and this corresponds to a 6.9% energy saving (from 0.0244 to 0.0227 kmol/s) over the conventional feed arrangement. Table 2 reveals that the two feeds move *away* from each other, and a little improved reactant composition distribution can be observed. In fact, the optimal feed trays are located quite close to the conventional feed trays (e.g., one and two trays away). An almost monotonic composition distribution in D is also observed and this leads to a little higher temperature in the lower section of the reactive trays but not by much. This explains why the improvement is not as significant as in the previous case.

3.2. Changing relative volatilities of products

Now let us consider the cases in which the relative volatilities of two products are different from the base case value of 2. Two cases are explored: one is that the light product (C) is easy to separate from the light reactant A (i.e., $\alpha_C/\alpha_A = 4$), and the other is that the relative volatility between the heavy reactant B and the heavy product D (i.e., $\alpha_B/\alpha_D = 4$) is larger than the base case value of 2.

In the first case, we have: $\alpha_C = 16$, $\alpha_A = 4$, $\alpha_B = 2$, and $\alpha_D = 1$. With the conventional feed arrangement, the energy consumption (0.0285 kmol/s) is 10.9% less than the base case because of the large relative volatility between C and A. Following the optimization procedure, the optimum feed trays become $N_{F,A} = 12$ and $N_{F,B} = 14$ (Fig. 7B). As compared to the conventional feed arrangement, this corresponds to a 46.8% energy saving (from 0.0285 to 0.0152 kmol/s)! This is a very significant energy saving by very simple means (feed rearrangement). Two observations can be made immediately. First, the two feeds are quite *close* to each other and the feed locations move to the upper section of the reactive zone. Second, the fraction of total conversion is distributed relatively uniform throughout the reactive zone (at least compared to other cases) as shown in Fig. 7B. This implies none of the reactive trays are under utilized, and they are achieved with the interplay between the composition and temperature distributions (e.g., showing temperature upturn whenever necessary). Again, an almost monotonic composition distribution in D can also be seen, and significantly smaller amount of the product C is also observed in the upper reactive zone, which allows for higher reactant concentration. All these factors result in much smaller vapor rate as compared to the conventional feed arrangement.

The other example is just the opposite in which we have an easy separation between the heavy reactant and the heavy product. In this case, the relative volatilities are $\alpha_C = 16$, $\alpha_A = 8$, $\alpha_B = 4$, and $\alpha_D = 1$, respectively. For

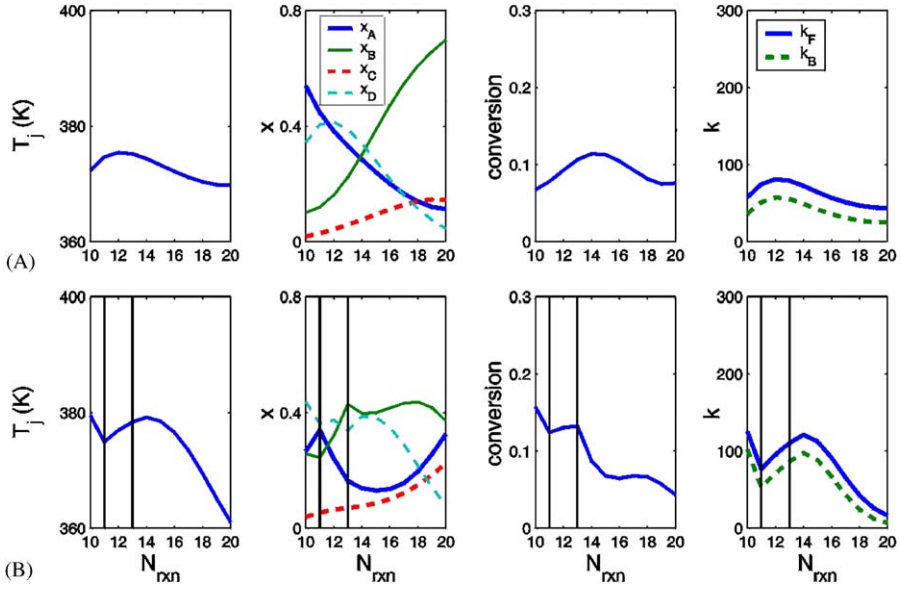

Fig. 6. Profiles of temperature, composition, fraction of the total conversion, and reaction rate constant in the reactive zone for the system $\alpha_C/\boldsymbol{\alpha_A}/\boldsymbol{\alpha_B}/\alpha_D = 6/\mathbf{3}/\mathbf{2}/1$ with: (A) conventional feed arrangement ($N_{F,A} = 10$ and $N_{F,B} = 20$), and (B) optimal feed arrangement ($N_{F,A} = 11$ and $N_{F,B} = 13$) with 15% energy saving.

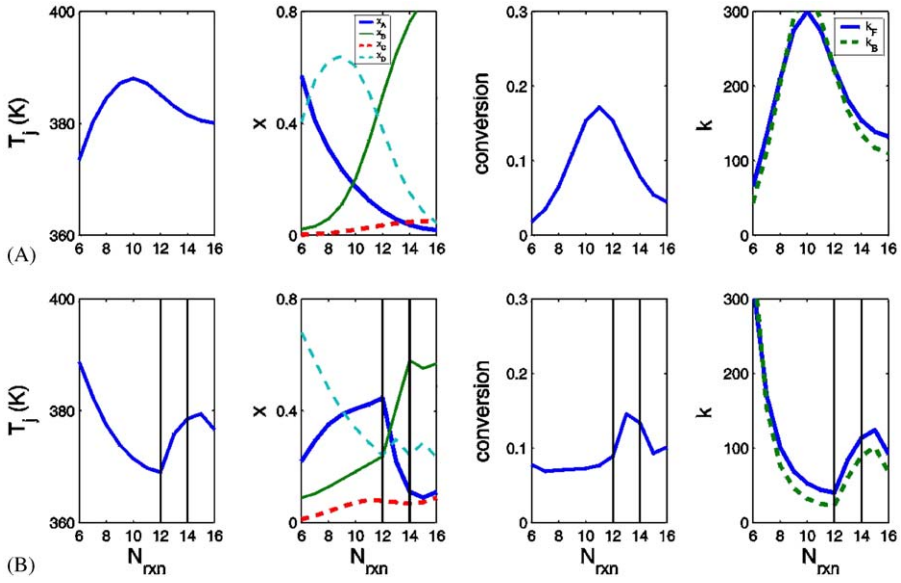

Fig. 7. Profiles of temperature, composition, fraction of total conversion, and reaction rate constant in the reactive zone for the system $\boldsymbol{\alpha_C}/\boldsymbol{\alpha_A}/\alpha_B/\alpha_D = \mathbf{16}/\mathbf{4}/2/1$ with: (A) conventional feed arrangement ($N_{F,A} = 6$ and $N_{F,B} = 16$), and (B) optimal feed arrangement ($N_{F,A} = 12$ and $N_{F,B} = 14$) with 46.8% energy saving.

the conventional feed arrangement, the energy consumption (0.0281 kmol/s) is only 87.8% of the base case. All these four cases confirm that the well-known fact of the conventional distillation—easy separation requires less energy—can also be applied to reactive distillation. It is also observed that the concentration of D is smaller toward the lower reactive zone as compared to the other two cases (cf. Figs. 5A and 8A), and this allows a higher reactant concentration in the same section. The optimization result shows that the optimum feed trays are $N_{F,A} = 8$ and $N_{F,B} = 10$ (Fig. 8B), and this corresponds to a 15.6% energy saving (from 0.0281 to 0.0237 kmol/s) over the conventional feed arrangement (Table 2). It is also observed that these two feeds are quite *close* to each other and they are located in the lower section of the reactive zone, as can be seen in Fig. 8B. In addition to an almost monotonic composition distribution in D, a

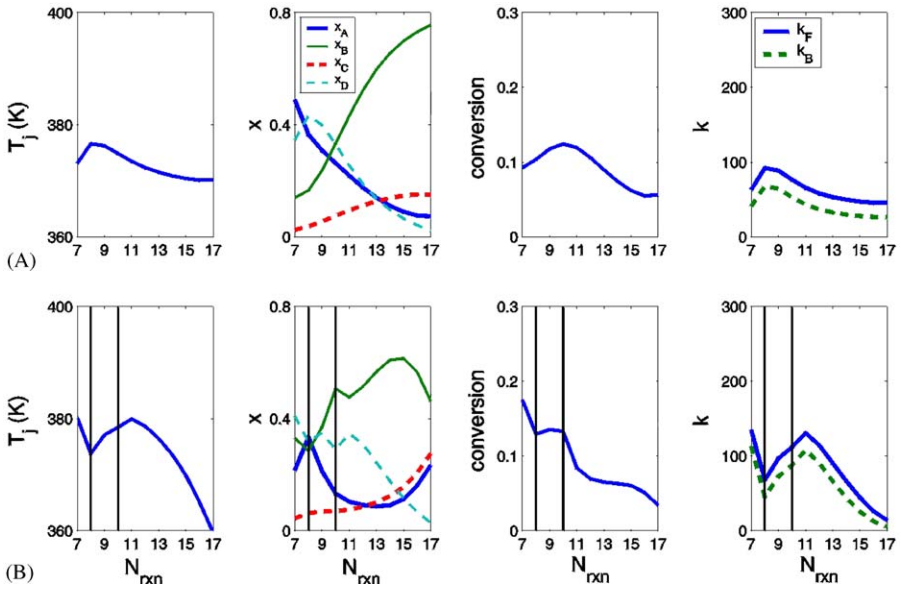

Fig. 8. Profiles of temperature, composition, fraction of total conversion, and reaction rate constant in the reactive zone for the system $\alpha_C/\alpha_A/\alpha_B/\alpha_D = \mathbf{16}/\mathbf{8}/4/1$ with: (A) conventional feed arrangement ($N_{F,A} = 7$ and $N_{F,B} = 17$), and (B) optimal feed arrangement ($N_{F,A} = 8$ and $N_{F,B} = 10$) with 15.6% energy saving.

high concentration of B throughout the reactive zone is also observed in Fig. 8B, and this improves the effectiveness of the reactive trays. This is allowed because B can be separated easily from the heavy product D. However, unlike in the previous case, the decreasing trend of the temperature toward the upper reactive zone leads to a monotonically decreasing fraction of total conversion in the same direction (Fig. 8B). The underutilized reactive trays in the upper reactive zone explain why the margin of improvement is not quite as significant as in the previous case.

3.3. Summary

On-going analyses clearly indicate that the feed locations are important design parameters, and significant energy saving (ranging from 7% to 47%) will result if we place the feed trays optimally (Table 2). As for the specific feed locations, the following heuristics are useful.

Heuristic H2. Place the light and heavy reactant's feed location *close* to each other when the relative volatility between the reactants is *small* (e.g., Fig. 6B). Similarly, move the feed tray locations *away* from each other when the relative volatility between the reactants is *large*.

Heuristic H3. When the relative volatility between the *light reactant and the light product is large*, move the feed locations *upward* (i.e., to the upper reactive zone; e.g., Fig. 7B). Similarly, when the relative volatility between the *heavy reactant and the heavy product is large*, move the feed locations *downward* (i.e., to the lower reactive zone; e.g., Fig. 8B).

These were observed not only for systems with base case kinetics (Table 2), but also for processes with temperature less sensitive kinetics (Table 3). Also note that the terms "small" and "large" used are in a relative sense.

4. Effects of reaction kinetics

In this section, the effects of reaction kinetics to the optimal feed tray locations to the corresponding energy saving are explored. Two scenarios are studied. One is the activation energies for both forward and backward reactions are reduced by an order of magnitude and this implies a less temperature-sensitive reaction rate. The other is the case where the pre-exponential factor is varied. We are interested in how these changes will impact the optimal feed locations and the corresponding percentage of energy saving.

4.1. Reducing activation energies

Consider the case in which the forward and backward activation energies are reduced to 3000 cal/mol, an order of magnitude smaller. In both cases, we fix the rate constants to 0.008 and 0.004 at 366 K for the forward and backward reactions (Table 1). This has two impacts to the reactive distillation. First, the reactions are not quite as temperature sensitive as in the previous case. Second, the heat of reaction is zero, as opposed to the previous case where 10 000 cal heat is released for every mole reactant converted.

Table 3
Effects of feed locations to design for systems with different relative volatilities (temperature insensitive kinetics; $E_F = 3000$ and $E_B = 3000$ cal/mol)

	Base case	$\frac{\alpha_A}{\alpha_B} = 2$	$\frac{\alpha_A}{\alpha_B} = 1.5$	$\frac{\alpha_A}{\alpha_B} = 3.0$	$\frac{\alpha_C}{\alpha_A} = 4.0$	$\frac{\alpha_B}{\alpha_D} = 4.0$
$\alpha_C/\alpha_A/\alpha_B/\alpha_D$	**8/4/2/1**	**8/4/2/1**	**6/3/2/1**	**12/6/2/1**	**16/4/2/1**	**16/8/4/1**
$k_{F,375}$ (s^{-1})	**0.0215**	0.0215	0.0215	0.0215	0.0215	0.008
$k_{B,375}$ (s^{-1})	**0.0150**	0.0150	0.0150	0.0150	0.0150	0.004
$N_S/N_{r\times n}/N_R$	7/11/8	7/11/8	8/11/8	8/11/8	5/11/6	6/11/6
$N_{r\times n,\text{bot}}/N_{r\times n,\text{top}}$	**8/18**	**8/18**	**9/19**	**9/19**	**6/16**	**9/19**
$N_{F,A}/N_{F,B}$	**8/18**	**11/15**	**13/15**	**10/17**	**14/15**	**9/12**
$X_{D,C}/X_{B,D}$	0.95/0.95	0.95/0.95	0.95/0.95	0.95/0.95	0.95/0.95	0.95/0.95
F_{OA} , F_{OB}, D, B (kmol/s)	0.0126	0.0126	0.0126	0.0126	0.0126	0.0126
R (kmol/s)	0.0267	0.0225	0.0264	0.0185	0.0105	0.0185
V_S (kmol/s)	0.0393	0.0351	0.0390	0.0311	0.0231	0.0311
Percent energy saving[a] (%)	**0**	**−10.7**	**−19.1**	**−5.4**	**−33.6**	**−14.7**

[a]Compared to the conventional feed arrangement (i.e., $N_{rxn,\text{bot}} = N_{F,A}$ and $N_{rxn,\text{top}} = N_{F,B}$).

4.1.1. Base case for the low activation energy example

With the conventional feed arrangement, the profiles of temperature, composition, and fraction of total conversion are qualitatively similar to that of the high activation example (Fig. 5A), except for the profile of the reaction rate where the low activation energy example exhibits a much lower rate for the backward reaction. However, the energy consumption is higher in the present example as compared to one with a higher activation energy (0.0393 versus 0.0320 kmol/s). The reason for that is that the heat is no longer released from the reactions, and the effect of direct heat integration disappears. Following the optimization procedure, the optimal feed trays becomes $N_{F,A} = 11$ and $N_{F,B} = 15$, and this results in a 10.7% energy saving, when compared to the conventional feed arrangement (Table 3). Similar to the example of high activation energy, these two trays are located 4 trays apart. But, unlike the previous case, the relative position moves up a little. This is within one's expectation because, here, we have a less temperature-sensitive reaction, and the effects of the temperature profile is not as important as in the previous example. This indicates that composition profile is much more important in this example. The fraction of total conversion on reactive trays clearly indicates a non-monotonic profile throughout the reactive zone, compared to the high activation energy case (Fig. 5B). The temperature insensitivity is also illustrated in the profile of the rate constants where the ratio of the maximum over the minimum rate constants is 1.3 in this case, while the high activation energy example gives a value of 22! In terms of energy saving via feed tray optimization, both cases show quite similar results (10.7% versus 10.9% as shown in Tables 2 and 3).

4.1.2. Changing relative volatilities of reactants

Similar to the previous example, first we explore the case of the difficult separation between the two reactants. The relative volatilities are $\alpha_C = 6$, $\alpha_A = 3$, $\alpha_B = 2$, and $\alpha_D = 1$, respectively. Following the optimization procedure, the optimal feed trays are $N_{F,A} = 13$ and $N_{F,B} = 15$, and a 19.1% energy saving (from 0.0482 to 0.0390 kmol/s) can be achieved by the feed re-arrangement (Table 3). It is clear that the heuristic H2 applies here, and the percentage of energy saved is quite similar to the high activation energy counterpart (Table 2).

Next, the case of difficult separation between reactants is examined. The relative volatilities are α_C=12, α_A=6, α_B=2, and α_D=1, respectively. The feed tray location optimization gives: $N_{F,A} = 10$ and $N_{F,B} = 17$. In this case, only 5.4% energy can be saved (from 0.0328 to 0.0310 kmol/s) because the conventional feed arrangement is a pretty good design to begin with (Table 3). Again, the heuristic H2 applies here, and the percentage of energy saved is also similar to the high activation energy counterpart (Table 2).

4.1.3. Changing relative volatilities of products

Following the high activation energy example, here, we study the case of an easy separation between the light reactant and the light product. The relative volatilities in this case are $\alpha_C = 16$, $\alpha_A = 4$, $\alpha_B = 2$, and $\alpha_D = 1$, respectively. Recall that this scenario results in the largest energy saving for the high activation energy case (Fig. 7B). Following the optimization procedure, the optimal feed trays are $N_{F,A}$=14 and $N_{F,B} = 15$, and a 33.6% energy saving (from 0.0348 to 0.0231 kmol/s) can be achieved by the feed re-arrangement (Table 3). Again, the heuristic H2 applies here, and the percentage of energy saved is quite significant but not quite as large as that of the high activation energy counterpart (33.6% versus 46.8%).

Finally, the case of easy separation between the heavy reactant and the heavy product is explored. The relative volatilities are $\alpha_C = 16$, $\alpha_A = 8$, $\alpha_B = 4$, and $\alpha_D = 1$, respectively. The feed tray location optimization gives: $N_{F,A} = 9$ and $N_{F,B} = 12$. In this case, 14.7% energy can be saved (from 0.0365 to 0.0311 kmol/s) (Table 3). Again, the heuristic H2 applies here, and the percentage of energy saved is also similar to the high activation energy counterpart (Table 2).

4.1.4. Summary

For the low activation energy kinetics, the reaction rate constants are relatively insensitive to temperature. Thus, the composition profile plays a more important role than the temperature profile. Again, the feed tray locations play an important role in design. Generally, the average percentage of energy saving is a little less than the high activation energy counterpart (cf. Tables 2 and 3). Again, this example clearly illustrates that heuristics H2 and H3 offer good guidelines to place the feeds.

4.2. Effects of pre-exponential factor

In this work, we change the pre-exponential factor of the rate expressions while fixing the activation energies to 30 000 and 40 000 cal/mol (the high activation energy case). The rate constants are reduced and increased at 366 K by adjusting the pre-exponential factors. These can be viewed as two different systems or the scenarios of changing catalyst activity. Again, the optimal feed tray location and percent of energy saving are of interest here.

4.2.1. Lower reaction rate constant

In this work, we consider a lower reaction rate constant with the following relative volatilities $\alpha_C/\alpha_A/\alpha_B/\alpha_D = 8/4/2/1$. The specific reaction rates at 366 K are changed to 60% of the nominal values, $k_F = 0.0048$ and $k_B = 0.0024$.

Because the reaction rates are almost 60% smaller, under the conventional feed arrangement, the vapor rate increases by a factor of 30% to meet product specifications as compared to the nominal case (Table 2). Here the product D takes a slightly lower value than the base case (Fig. 5A), and more energy is required to separate the product from the reactants. Following the optimization procedure, the optimal feed locations are: $N_{F,A} = 9$ and $N_{F,B} = 17$. This results in only a 5.5% energy saving (Table 2). Fig. 9 shows the profiles of temperature, composition, conversion, and rate constants in the reactive zone. Because of smaller rate constants, the reactants do not decrease as fast as the case of high rate constants (e.g., Fig. 5A). In fact, a favorable reactant compositions profile is observed, and this is essential for good performance. In other words, the conventional feed arrangement is already a good choice, and the optimized feed trays provide a little improvement in the reactant distribution.

4.2.2. High reaction rate constant

In this case, the reaction rate constants are doubled at 366 K (i.e., $k_F = 0.016$ and $k_B = 0.008$). Because of higher reaction rates, the numbers of trays in the stripping and rectifying sections decrease, and in addition, the vapor rate is also reduced by a factor of 8%. With the conventional feed arrangement, the reactant compositions decrease drastically toward the opposite ends of the reactive zone as shown in Fig. 9A. These are not favorable profiles from the reaction standpoint. It is expected that optimizing the feed traylocation can reduce operating cost. Following the procedure, the optimal feed trays are: $N_{F,A} = 10$ and $N_{F,B} = 13$ (Fig. 9B). This results in a 21.9% saving in the vapor rate which is quite significant as compared to that of the base case (Table 2). It is also observed that the fractional conversion is distributed relatively uniform throughout the reactive section, compared to the conventional feed arrangement.

4.2.3. Summary

We gain some insight by studying these three systems with low (60%), nominal (100%), and high (200%) rate constants. First, as expected, the energy consumption goes up as the rate constant becomes smaller (Table 2), and this is true for either the conventional feed arrangement or the optimized feed locations. Second, the percentage of the energy saved by optimizing the feed locations increases up as the rate constant becomes larger. The reason for that is that the shapes of reactant profiles are not favorable for reaction when the rate constants are large under the conventional feed arrangement. Third, the optimal feed trays move closer to each other when the rate constants go up. This results in the following heuristic:

Heuristic H4. Place the feed trays *away from each other* when the rate constants become *smaller*. Similarly, move the feed tray locations *closer to each other* when the rate constants become *larger* (e.g., Fig. 9B).

This heuristic is useful in design as well as for operation when the reaction rate constants vary.

5. Operation and control

On-going analyses clearly show that improved design can be achieved by treating the feed tray location as an optimization variable and results indicate that significant energy saving can be obtained by simply rearranging the feeds. However, these analyses are limited to the design aspects with different thermodynamics parameters (i.e., relative volatilities) as well as kinetics parameters (i.e., activation energy and pre-exponential factor). In this section, we are more interested in how this finding will affect the operation and the control of reactive distillation.

Despite clear economic incentives of reactive distillation, only a few papers studying the dynamics and control of reactive distillation have been published. Al-Arfaj and Luyben (2000) give a review on the closed-loop control of reactive distillation. Several control structures for an ideal two-product reactive distillation system and real chemical systems (Al-Arfaj and Luyben, 2002, 2004; Huang et al., 2004) have been proposed. One important principle in the control of reactive distillation is that we need to control one

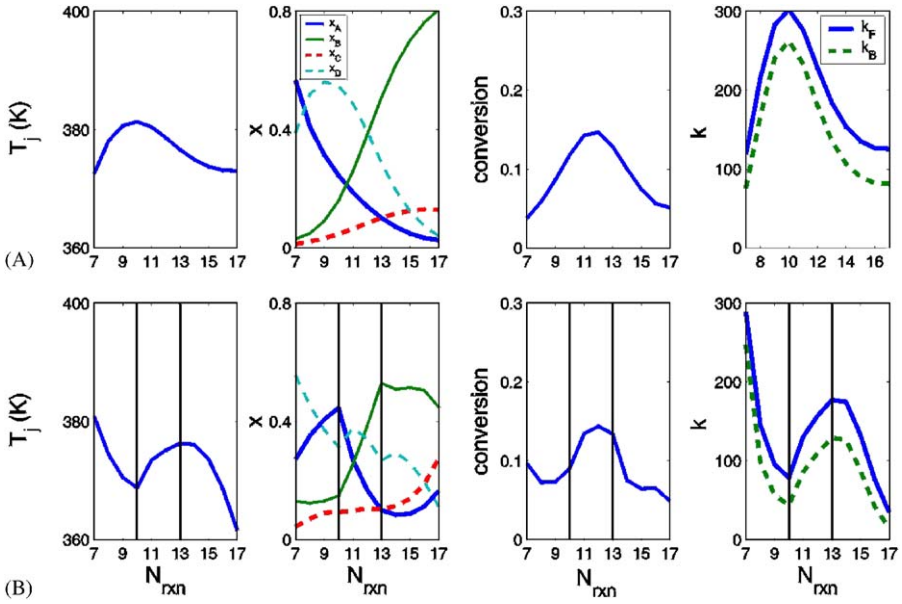

Fig. 9. Profiles of temperature, composition, fraction of total conversion, and reaction rate constant in the reactive zone for the system $\alpha_C/\alpha_A/\alpha_B/\alpha_D = 8/4/2/1$ when rate constants increased to 200% with: (A) conventional feed arrangement ($N_{F,A} = 7$ and $N_{F,B} = 17$), and (B) optimal feed arrangement ($N_{F,A} = 10$ and $N_{F,B} = 13$) with 22% energy saving.

intermediate composition (or tray temperature) in order to maintain stoichiometric balance (Al-Arfaj and Luyben, 2000).

5.1. Optimal feed location under production rate variation

In general, production rate variation is one of the most important load disturbance in plantwide control and operation (Luyben et al., 1999), and more importantly, it can be measured. In this work, we are interested in whether significant energy saving can be obtained by adjusting the feed tray locations as the production rate changes. If appreciable amount of operating cost can be reduced, the feed tray location is not only dominant design variable but useful manipulated variable for control.

Let us take the base case (Table 2) as an example, the optimal feed trays are: $N_{F,A} = 11$ and $N_{F,B} = 15$ as shown in Fig. 5B. The control objective is to maintain the product compositions (C and D) at 95%. Both positive and negative production rate variations are explored. First, consider the case with +40% feed flow rate increase. The optimization is performed to find the optimal feed locations by minimizing the vapor rate. One obtains $N_{F,A} = 10$ and $N_{F,B} = 16$ and this corresponds to a 28% of energy saving! This is not totally unexpected, because an increasing the production can be viewed, in a sense, as a short of reaction capability. The closest scenario to this situation is a decrease in the rate constant. Therefore, we should move the feed trays away from each other as suggested by heuristic H4. But the percentage of energy saving is larger than our expectation, because we do not explore the non-optimal cases in Section 4 (what if the feed locations are placed incorrectly). The findings here clearly show that the optimal feed trays can change as the feed rate varies. Next, the optimization is carried out for a −40% change in the feed flow rate. The optimal feed trays become $N_{F,A} = 12$ and $N_{F,B} = 15$ and a 9% saving in the vapor rate is observed. As pointed out earlier, this has the same effect as that from reaction rate increases, and one should moves the feed trays closer to each other. The results clearly indicate that one should change the feed tray locations as the production rate changes, because 9 or 28% energy can be saved by simply moving the feed trays. The next question then becomes how can we implement such a control strategy? The coordinated control of Doukas and Luyben (1976) offers some light in this direction (Chang et al., 1998).

5.2. Control structure

Before getting into the feed rearrangement control structure, let us first construct the fundamental control configuration for the reactive distillation with two feeds. Recall that, unlike the control of conventional distillation, one needs to control an internal composition (or temperature) to maintain stoichiometric amounts of the two fresh feeds (Al-Arfaj and Luyben, 2000). For the purpose of illustration, in this work, we choose to control composition of the reactant A on tray 13 where a large change in the composition A is observed (Fig. 5B). Thus, we have three compositions to be controlled, top composition of C, bottoms composition of D and composition A on tray 13. For the manipulated variables, the ratio scheme (Chiang et al., 2002) is used, and these three ratios are: reflux ratio, boilup ratio, and feed

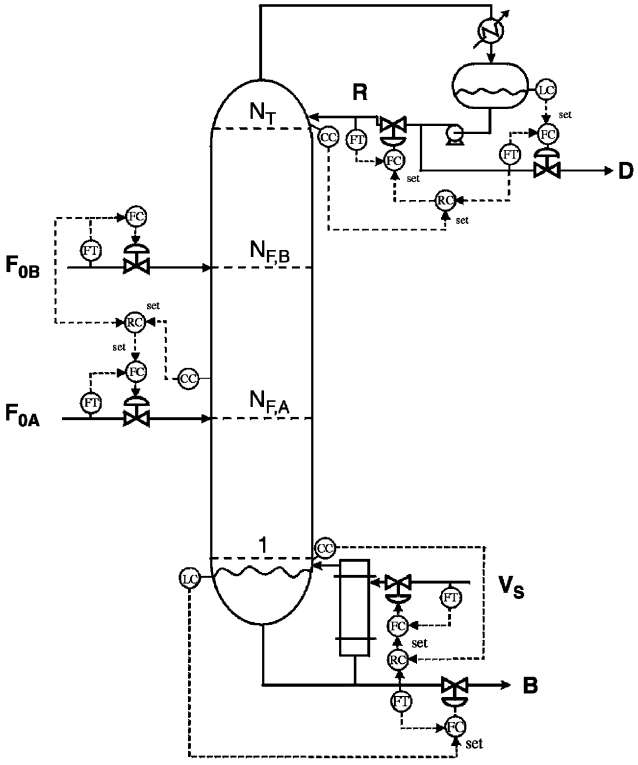

Fig. 10. Control structure of reactive distillation with fixed feed locations.

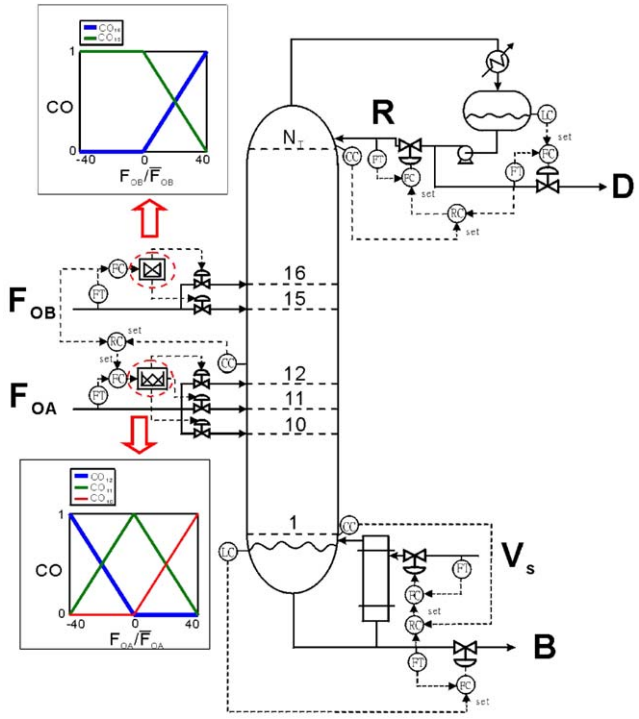

Fig. 11. Control structure of reactive distillation with coordinated feed locations as the production rate changes.

ratio. The steady-state sensitivity analysis gives the following steady-state gain matrix between the controlled and manipulated variables:

$$\begin{bmatrix} x_A \\ x_{D,C} \\ x_{B,D} \end{bmatrix} = \begin{bmatrix} 20.61 & 7.53 & -8.94 \\ 0.2 & 0.18 & -0.1 \\ 0.32 & -0.13 & 0.26 \end{bmatrix} \begin{bmatrix} F_{OA}/F_{OB} \\ R/D \\ V_S/B \end{bmatrix}.$$

The relative gain array (RGA, Λ) can be computed from the gain matrix.

$$\Lambda = \begin{matrix} \\ x_A \\ x_{D,C} \\ x_{B,D} \end{matrix} \begin{matrix} \begin{matrix} F_{OA}/F_{OB} & R/D & V_S/B \end{matrix} \\ \begin{bmatrix} 0.85 & -0.78 & 0.93 \\ -0.20 & 1.83 & -0.63 \\ 0.35 & -0.05 & 0.7 \end{bmatrix} \end{matrix}.$$

The result of the RGA indicates that one should pair the internal composition with the feed ratio, pair the top composition with reflux ratio, and pair the bottoms composition with boilup ratio ($x_A - F_{OA}/F_{OB}$, $x_{D,C} - R/D$, and $x_{B,D} - V_S/B$). After the variable pairing, the basic control loops are in place. Fig. 10 shows the control configuration for the reactive distillation without feed rearrangement.

(1) The fresh feed F_{OB} is the throughput manipulator which is flow control.
(2) F_{OA} is ratioed to F_{OB}, and the ratio is set by the tray 13 composition (x_A).
(3) The top composition of C is maintained by changing the reflux ratio.
(4) The bottoms composition of D is controlled by changing the boilup ratio.
(5) The base level is controlled by manipulating bottoms flow rate.
(6) The reflux drum level is maintained by adjusting the distillate flow rate.

This structure consists of 3 composition loops and 2 level loops. In this paper, decentralized control structure with PI controllers is employed for the composition loops, and perfect level control is assumed for the level loops. In the identification phase, the relay feedback method (Yu, 1999) is used to obtain the ultimate gain and ultimate period and the controllers are tuned using the Tyreus–Luyben turning method (Tyreus and Luyben, 1992). Note that five minutes of analyzer dead time was assumed for the composition measurement.

Because both fresh feed flows are measured, one can coordinate the feed location as the production rate changes. Let us take the upper feed flow as an example to illustrate the feed rearrangement. Nominally, the feed tray for the heavy reactant is tray 15, and as the flow rate (F_{OB}) increases by a factor of 40%, the feed location should be switched to tray 16. Thus, the idea is to use the feed tray location as a manipulated variable as the feed flow changes (Doukas and Luyben, 1976). Instead of making discontinuous switch, a linear combination of valve opening between trays 15 and 16 is in placed and this provides a gradual transition as the feed flow rate increases. Let us use the fresh feed of B, F_{OB}, to

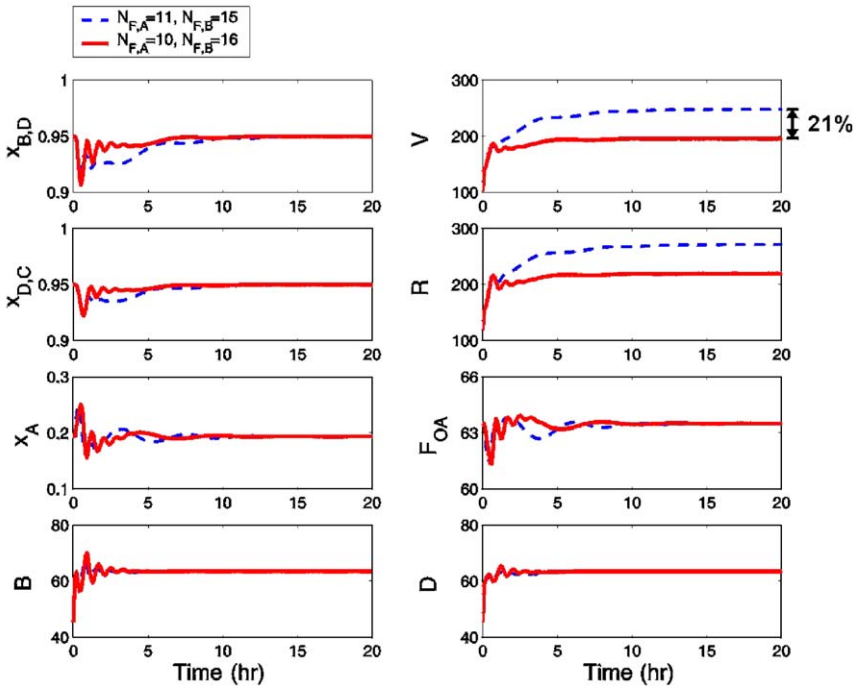

Fig. 12. Closed-loop responses for a +40% production rate increase with fixed feed locations (dashed) and coordinated feed trays (solid).

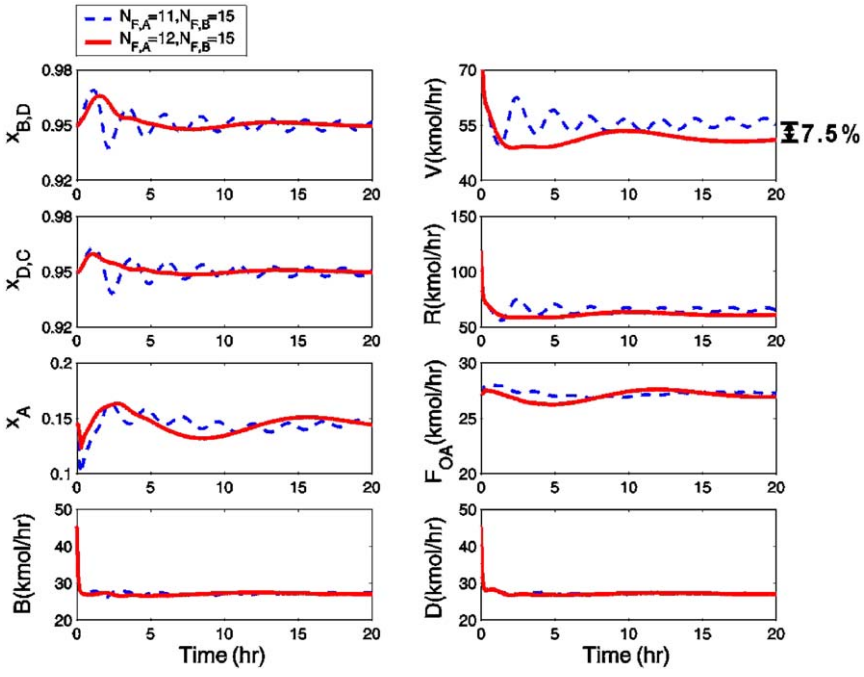

Fig. 13. Closed-loop responses for a 40% production rate decrease with fixed feed locations (dashed) and coordinated feed trays (solid).

illustrate the coordination between the valve openings into tray 15 and 16. At nominal flow rate ($F_{OB}/\bar{F}_{OB} = 0$ in the box in the upper corner of Fig. 11), only valve to tray 15 is open, while the valve to tray 16 is shut. As the feed flow rate increases (i.e., $F_{OB}/\bar{F}_{OB} > 0$), the valve to tray 16 is open gradually, while closing the valve to tray 15. When the feed flow rate reaches 40% increase ($F_{OB}/\bar{F}_{OB} = 0.4$), only the valve to tray 16 remains open, and the valve to tray 15 is totally closed. This provides a mechanism to coordinate the openings of these two valves. The same idea can be extended to the feed flow of A, switching between trays 10, 11, and 12 as shown in the lower box in Fig. 11. This can be

implemented in distributed control system (DCS) with little difficulty.

5.3. Closed-loop performance

Next, the closed-loop performance of both control structures (with and without feed rearrangement) is evaluated (Figs. 10 and 11). First, consider the case of a 40% production rate increase. The control structure with coordinated control (Fig. 11) gives fast dynamics in the product composition, as can be seen in Fig. 12 where top and bottoms composition return to set point in less than 10 h (solid line in Fig. 12). On the other hand, the conventional control structure (Fig. 10) shows a little slower dynamic responses and the product compositions do not return to the set points after 10 h. More importantly, the coordinated control structure results in a 21% energy, compared to the conventional control structure, which can be seen from the smaller vapor rate in Fig. 12. Note that a 21% energy saving is smaller than a 28% from steady-state analysis, and the reason is that we fix the tray 13 composition of A to the nominal value. Nonetheless, the amount of energy saved is still quite significant. Fig. 13 shows the responses for −40% step changes in the production rate. Again, faster dynamics for top and bottoms products are observed for the coordinated control structure (Fig. 11). Moreover, a 7.5% energy saving can be achieved with this improved dynamics.

The results presented in this section clearly show that the concept of optimal feed tray location can be carried over to process operation and control. With a simple modification in the control structure (Fig. 11), improved closed loop performance can be achieved with substantial energy saving.

6. Conclusion

In this paper, the effects of feed locations to the design of reactive distillation are explored, and ideal reactive distillation systems are used to illustrate the advantage of feed trays optimization. Reactive distillation columns with various process parameters were explored. They include: relative volatilities between reactants, relative volatilities between products, column pressure, activation energies, and pre-exponential factors. The results from all system studied indicates a 6% to 47% energy saving, which can be achieved by simply rearrange the feed locations. Because the temperature and composition profiles play a vital role for the effective utilization of the reactive section, the optimal feed locations are essential to obtain improved performance. Qualitatively, heuristics are also given to place the feeds at the vicinity of optimal locations. Quantitatively, a systematic procedure is proposed to find the right feed trays. Finally, the idea of optimal feed trays can be carried over to the control of reactive distillation system. First, steady-state analysis is performed to find the optimal feed trays as the measurable load variable changes. Then, a coordinated control structure is proposed to rearrange the feeds as the disturbance comes into the system. The results indicate that, again, substantial energy can be saved during process operation by feed rearrangement while showing improved closed-loop dynamics.

Notation

a_B	pre-exponential factor for the reverse reaction (kmol/s/kmol)
a_F	pre-exponential factor for the forward reaction (kmol/s/kmol)
A	light reactant
B	heavy reactant
B	bottoms flow rate (kmol/s)
C	light product
CO	normalized controller output (between 0 and 1)
CO_j	fraction of valve opening to tray j (implying fraction of total feed flow to tray j)
D	heavy product
D	distillate flow rate (kmol/s)
E_B	activation energy of the reverse reaction (cal/mol)
E_F	activation energy of the forward reaction (cal/mol)
F_j	feed flow rate on tray j (kmol/s)
F_{OA}	fresh feed flow rate of reactant A (kmol/s)
F_{OB}	fresh feed flow rate of reactant B (kmol/s)
k_{Bj}	specific reaction rate of the reverse reaction in tray j (kmol/s/kmol)
k_{Fj}	specific reaction rate of the forward reaction in tray j (kmol/s/kmol)
L_j	liquid flow rate from tray j (kmol/s)
M_j	liquid holdup on tray j (kmol)
$N_{F,A}$	number of fresh feed A tray
$N_{F,B}$	number of fresh feed B tray
$N_{r\times n}$	number of reactive trays
N_R	number of rectifying trays
N_S	number of stripping trays
P	total pressure (bar)
P_i^S	vapor pressure of component i (bar)
R	reflux flow rate (kmol/s)
R	perfect gas law constant (cal/mol/K)
$R_{j,i}$	reaction rate of component i on tray j (kmol/s)
T_j	temperature in tray j (K)
V_j	vapor flow rate from tray j (kmol/s)
V_j	vapor flowrate in the stripping section (kmol/s)
$x_{j,i}$	composition of component i in liquid on tray j (mole fraction)
$y_{j,i}$	composition of component i in vapor on tray j (mole fraction)
$z_{j,i}$	composition of component i in feed on tray j (mole fraction)

Greek letters

α	relative volatility
β	liquid hydraulic time constant (s)
ΔH_v	heat of vaporization (cal/mol)
λ	heat of reaction (cal/mol of C produced)
Λ	relative gain array
v_i	stoichiometric coefficient of the ith component

Superscript

$-$	nominal steady-state value

Acknowledgements

This work was supported by the National Science Council of Taiwan under Grant NSC 93-2214-E002-013 and YCC was supported in part by the Ministry of Economic Affairs under Grant 92-EC-17-A-09-S1-019.

References

Al-Arfaj, M.A., Luyben, W.L., 2000. Comparison of alternative control structures for an ideal two-product reactive distillation column. Industrial and Engineering Chemistry Research 39, 3298–3307.

Al-Arfaj, M.A., Luyben, W.L., 2002. Comparative control study of ideal and methyl acetate reactive distillation. Chemical Engineering Science 57, 5039–5050.

Al-Arfaj, M.A., Luyben, W.L., 2004. Plantwide control of TAME production using reactive distillation. A.I.Ch.E. Journal 50, 1462–1473.

Chang, D.M., Yu, C.C., Chien, I.L., 1998. Coordinated control of blending systems. IEEE Transactions Control System Technology 6, 495–506.

Chiang, S.F., Kuo, C.L., Yu, C.C., Wong, D.S.H., 2002. Design alternatives for amyl acetate process: coupled reactor/column and reactive distillation. Industrial and Engineering Chemistry Research 41, 3233–3246.

Doherty, M.F., Buzad, G., 1992. Reactive distillation by design. Transactions of the Institution of Chemical Engineers, Part A 70, 448–458.

Doherty, M.F., Malone, M.F., 2001. Conceptual Design of Distillation Systems. McGraw-Hill, New York.

Douglas, J.M., 1988. Conceptual Process Design. McGraw-Hill, New York.

Doukas, N., Luyben, W.L., 1976. Control of sidestream columns separating ternary mixtures. Instrumentation Technology 25 (6), 43–48.

Huang, S.G., Kuo, C.L., Hung, S.B., Chen, Y.W., Yu, C.C., 2004. Temperature control of heterogeneous reactive distillation: butyl propionate and butyl acetate esterification. A.I.Ch.E. Journal 50, 2203–2216.

Kaymak, D.B., Luyben, W.L., 2004. A quantitative comparison of reactive distillation with conventional multi-unit reactor/column/recycle systems for different chemical equilibrium constants. Industrial and Engineering Chemistry Research 43, 2493–2507.

Kaymak, D.B., Luyben, W.L., Smith IV, O.J., 2004. Effect of relative volatility on the quantitative comparison of reactive distillation and conventional multi-unit systems. Industrial and Engineering Chemistry Research 43, 3151–3162.

Luyben, W.L., 2000. Economic and dynamic impact of the use of excess reactant in reactive distillation systems. Industrial and Engineering Chemistry Research 39, 2935–2946.

Luyben, W.L., Tyreus, B.D., Luyben, M.L., 1999. Plantwide Process Control. McGraw-Hill, New York.

Sundmacher, K., Kienle, A., 2003. Reactive Distillation. Wiley-VCH, Weinheim, Germany.

Sundmacher, K., Qi, Z., 2003. Conceptual design aspects of reactive distillation processes for ideal binary mixtures. Chemical Engineering and Processing 42, 191–200.

Taylor, R., Krishna, R., 2000. Modelling reactive distillation. Chemical Engineering Science 55, 5183–5229.

Tyreus, B.D., Luyben, W.L., 1992. Tuning PI controllers for integrator/dead time processes. Industrial and Engineering Chemistry Research 31, 2625–2628.

Yu, C.-C., 1999. Autotuning of PID Controllers. Springer, London.